Scripta Materialia 127 (2017) 15–18

Contents lists available at ScienceDirect

Scripta Materialia

journal homepage: www.elsevier.com/locate/scriptamat

Regular Article

Experimentally validated dwell and cyclic fatigue crack nucleation model for α–titanium alloys

D. Ozturk [a], A.L. Pilchak [b], S. Ghosh [a,*]

[a] Departments of Civil and Mechanical Engineering, Johns Hopkins University, Baltimore, MD 21218, United States
[b] Air Force Research Laboratory, Materials and Manufacturing Directorate (AFRL/RXCM), Wright Patterson AFB, OH 45433, United States

ARTICLE INFO

Article history:
Received 14 July 2016
Received in revised form 23 August 2016
Accepted 24 August 2016
Available online 6 September 2016

Keywords:
Ti-7Al alloy
Probabiltiy-based crack nucleation model
Image-based crystal plasticity FEM
Experimental observations
Dwell and cyclic loading

ABSTRACT

This paper develops an experimentally calibrated and validated crystal plasticity finite element model with a probabilistic crack nucleation model for predicting dwell and cyclic fatigue crack nucleation in polycrystalline microstructures of titanium or Ti alloys. The nucleation model accounts for load-shedding due to time-dependent plastic flow and variability in crystal strength. The predictions are corroborated with experimental observations of nucleation times for dwell and cyclic loading. Experimental characterization of failed samples reveal that crack initiation on (0001) planes are highly inclined away from the stress axis. The probability distribution of simulated facet orientations are in agreement with experimentally measured orientations.

1. Introduction

Titanium alloys, with low-symmetry hexagonal closed packed (*hcp*) crystallographic structure, are widely used in structural and propulsion applications on account of superior mechanical properties. Under conditions of high mean stress or sustained peak loads in dwell cycles, *soft* grains oriented favorably with respect to stress state can creep substantially at lower temperatures. Large differences in the critical resolved shear stress (CRSS) between contiguous *hard* and *soft* grains result in grain boundary load-shedding with continuous stress increase in the hard grains [1,2]. This phenomenon can potentially result in large reductions in the cycles to crack nucleation [3–6]. Recent studies [7–9] suggest that strain-rate sensitivity may contribute to the dwell problem. Localization leading to crack nucleation is facilitated by the planarity of dislocation glide in high-Al-content Ti alloys, which is attributed to the presence of short range order and shearing of coherent α_2 precipitates [10,11]. Dislocation pile-up at grain boundaries lead to stress concentrations in the adjacent grain in pure Ti [12], which leads to fracture unless relaxed by slip transmission or source-activation mechanisms [12–14]. Fracture surfaces of failed Ti alloy samples have a characteristic faceted appearance, formed by transgranular fracture across primary α-grains and/or the transformed β phase. Crack nucleation is observed to occur first at boundaries between α-grains that have their [0001] axis nearly parallel (*hard* grain) and nearly perpendicular (*soft* grain) to the principal stress axis respectively. These grains form faceted cracks that are inclined at ~15° and parallel to the (0001) plane [15,16]. The faceted fracture surface formation in dwell-fatigued Ti is accompanied by large reductions in fatigue life from reduced nucleation life and accelerated crack growth [15]. Experimental investigations on dwell fatigue [17,18] suggest that primary sub-surface crack nucleation can occur as late as ~80–90% of the total cycles to failure.

Several modeling approaches are proposed for prediction of crack nucleation. A Cellular Automata model [19] allows grain-scale analysis of accumulated stress and strain over large number of grains. Using image-based crystal plasticity finite element (CPFE) modeling of statistically equivalent representative volume elements (SERVE) of polycrystalline microstructures, a deterministic fatigue crack nucleation criterion is developed in [1,2]. The crack-nucleation model incorporates load-shedding induced stress concentrations in the hard grain and dislocation pile-up in the neighboring soft grain. To account for stochastic distribution of defects and their evolution near grain boundaries, a probabilistic extension of the deterministic model in [1,2] is developed in this paper. The model is validated with experiments for the number of cycles to nucleation and the local character of the nucleated sites. While the present physics-based approach provides a viable crack nucleation model, there are emerging alternative robust approaches [19,20].

2. Experimental studies

Experimental studies are performed on a single-phase binary titanium alloy with composition Ti-7Al-0.08O-0.05Fe. The material is prepared by casting and hot isostatic pressing a 76-mm round ingot

* Corresponding author.
E-mail address: sghosh20@jhu.edu (S. Ghosh).

http://dx.doi.org/10.1016/j.scriptamat.2016.08.031
1359-6462/

followed by extrusion at 7:1 ratio. The material is annealed at 955 °C for 24 h followed by furnace cooling to produce a fully recrystallized microstructure with 100 μm average. Samples with a gage volume of 317.5-mm^3 are cut transverse to the extrusion direction so the texture has an equal density of basal poles 0°-90° from the stress axis. Cyclic (0.5-Hz) and dwell fatigue (2-min hold) tests are performed at 85% and 100% of the alloy yield strength (662 MPa) with $R = 0.1$. Approximate number of cycles to crack initiation is determined by periodically interrupting dwell fatigue tests and performing X-ray computed tomography and also by using a fracture mechanics model to subtract the crack growth lifetime [21] (Table 1). Electron backscatter diffraction (EBSD) scans from a 254-mm^2 area are used to generate SERVE using the DREAM.3D software [22].

Various microstructural features are responsible for dwell fatigue crack nucleation in polycrystalline Ti alloys. Discontinuities in elastic stiffnesses across the boundaries of micro-textured regions (MTR) cause large stresses at these interfaces leading to conditions that favor crack nucleation [4,5]. Creep in plastically softer regions also amplifies stresses in adjacent hard regions. The potential for nucleation at length-scales of ~15–20-μm, is high at regions of amplified stress in the hard MTR. TEM observations reveal extensive basal <a> glide on parallel planes in the soft grain leading to the formation of extended pileup structures. These parallel basal slip systems are spanned by {10−11}<11−23> dislocations that increase in density near the initiation site. The adjacent hard grain also shows evidence of basal <a> slip with very extensive <c+a> slip. Experimental observations in [15,16] indicate that the microcrack formed in the grain boundary propagates back down the (0001) slip plane in the soft grain and also on a plane inclined at ~15° to the (0001) direction in the hard grain, thus forming two unique facets on the fracture surface.

3. Image-based crystal plasticity finite element model for fatigue crack nucleation

Size- and rate-dependent image-based crystal plasticity finite element (CPFE) models of deformation leading to fatigue crack nucleation in polycrystalline Ti alloys are developed in [1,2,23–25]. Microstructural length-scale and crystallographic effects on load shedding are incorporated in [25,26]. A deterministic, nonlocal crack nucleation criterion is developed in [1,2], which accounts for: (i) the normal and shear stress rise in hard grain, and (ii) dislocation pile-up due to time-dependent plastic strain in the neighboring soft grains. This dual dependence allows the model to naturally transcend situations, where the fatigue cracking is predominantly stress-controlled to those that are controlled by the effective strain. Consequently, the model is expected to have predictive capabilities for both dwell and cyclic fatigue loadings. The models in [1,2] however do not account for the local variability in crystal strength due to stochastic dispersion of defects at the length-scale of dislocation structures and pileups [16]. This is remedied in this paper through a probabilistic extension of the deterministic model to account for the defect variability and their cyclic evolution. An important predictive feature of this model is that it naturally solves for the plane of fatigue crack nucleation and does not force it to a pre-defined crystallographic plane. The image-based CPFE model is coupled with a powerful wavelet transformation induced multi-time scale (*WATMUS*) integration algorithm [2,27], which enables rapid traversal of a large number of cycles in high-fidelity micro-mechanical analyses, necessary for predicting fatigue failure. This WATMUS model is indispensable due to the large number of cycles before nucleation.

Table 1
Comparison of experimentally observed and simulated number of cycles to crack nucleation at varying peak loads $\mathbf{P_{max}}$, % error in calculated cycles with respect to observed values and dwell debits.

	Experimental cycles			Simulation cycles		
P_{max} (% of Y.S.)	Dwell	Cyclic	Dwell debit	Dwell (error)	Cyclic (error)	Dwell debit
100	~2500	~15,000	~6	2547 (2%)	13,941 (7%)	5.5
85	~21,000	~43,000	~2	22,915 (9%)	36,352 (15%)	1.6

4. A probabilistic fatigue crack nucleation model

A nonlocal fatigue crack nucleation model is proposed in [1,2] that captures the effects of both the stress rise due to load shedding and increasing plastic strain in adjacent grains. As shown in Fig. 1, the crack nucleation model is built on the premise that a wedge crack nucleates in the hard grain as dislocations approach and pile-up at the grain boundary of a soft grain. An edge dislocation is equivalent to a microcrack with opening displacement of one atomic spacing. As more dislocations pile up, the opening displacement increases in size. The crack opening displacement corresponds to the closure failure along a circuit surrounding the piled-up dislocations. The wedge crack is consistent with propagation back into the soft grain, as reported in experiments [9,10].

Cracks nucleate from the tip, when the mixed-mode stress intensity factor K_{mix} exceeds a critical fracture toughness value K_c. The multi-axial stress on the micro-crack surface is a combination of normal and shear stresses, represented by an effective traction as $T_{eff} = \sqrt{\langle T_n \rangle^2 + \beta T_t^2}$, where T_n and T_t are normal and shear components of the traction on the crack plane with a normal $\hat{\mathbf{n}}^{cra}$. The term $\langle T_n \rangle$ in the Macaulay bracket assures that compressive stresses do not contribute to crack opening. β is a shear stress factor that assigns different weights to the normal and shear traction components for mixed-mode and is defined as the ratio of the shear to normal fracture toughness as: $\beta \approx K_{IIc}/K_{Ic}$. The dislocation pile-up length is assumed to scale with the pre-crack length in crack tip nucleation models. Analogously, the hard grain crack nucleation criterion, ahead of dislocation pile-ups in adjacent soft grains has an inverse square root dependence on the equilibrated length c of the wedge-shaped microcrack shown in Fig. 1. The criterion is stated as:

$$T_{eff} = \sqrt{\langle T_n \rangle^2 + \beta T_t^2} \geq \frac{K_c}{\sqrt{\pi c}} = \frac{R_c}{\sqrt{c}}, \text{ or equivalently } . \quad R = T_{eff} \cdot \sqrt{c} \geq R_c \tag{1}$$

where R is a nucleation parameter and $R_c = K_c/\sqrt{\pi}$ is its critical value representing the nucleation strength that depends on the elastic properties, as well as on the critical strain energy release rate $\mathcal{G}_c$. It has the units of stress intensity factor (MPa$\sqrt{\mu m}$). The equilibrated length c is related to the edge dislocation pile up length B in the soft grain using the relation $c = \frac{G}{8\pi(1-\nu)\gamma_s} B^2$ given in [1,28]. G is the shear modulus and γ_s is the surface energy.

The parameter R is calculated at every finite element node that lies on the shared boundaries of contiguous grain pairs. The traction is

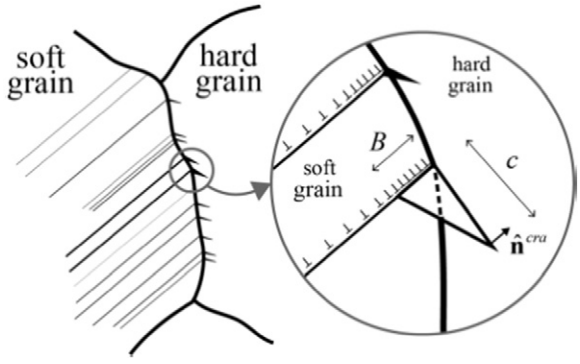

Fig. 1. A schematic of nucleation of a wedge crack with opening displacement of B resulting from a dislocation pileup in the soft grain.

calculated using the stress tensor at the node, derived from the stress field in the hard grain. As shown in Fig. 1 the microcrack with a normal $\hat{\mathbf{n}}^{cra}$ is nearly perpendicular to the net Burgers vector $\boldsymbol{B}$. The dislocation pile up length B, is calculated by integrating Nye's dislocation tensor, which is calculated as the curl of the plastic deformation gradient $\boldsymbol{\Lambda} = \nabla \times \boldsymbol{F}^p$, over a planar surface with normal $\hat{\mathbf{n}}$ bounded by a Burgers circuit around the node and inside the soft grain. The nucleation parameter R is calculated for 4615 Burgers circuits in this study, such that their surface normals uniformly sample the unit sphere at 3° resolution, and the largest value of R is taken to govern nucleation for the node.

To account for stochastic defect distribution, a probabilistic extension of the crack nucleation model is made by considering R_c as a random variable. Its local value may depend on the dislocation debris, point defect density and impurity content near the boundary of the hard grain. The probability of a microcrack nucleation in the hard grain is expressed using Eq. (1) as $P^{nucl} = P(R > R_c)$. As shown in Fig. 1, a large number of dislocation pileups along slip systems impinge on the grain boundary. To accommodate this, a slip band density is defined as $\rho_d = 1/A_d$, where A_d represents the effective cross section area of each slip band impinging on the grain boundary. The evolution of slip band thickness A_d with load cycles N_c is modeled using an exponential relation: $A_d(N) = A_{d,0} e^{N/N_c}$, where $A_{d,0}$ is the initial thickness of thin diffuse slip bands and N_c is a scaling parameter to control the growth rate in the exponential model. The value of $A_{d,0}$ is estimated as $0.001\,\mu m^2$, while N_c is calibrated from observations of the number of cycles to nucleation. In the numerical implementation, the grain boundary surfaces are divided into representative areas A_i^{eff} around each boundary node i using Voronoi tessellation. The number of potential microcracks that can nucleate around each boundary node is $N_i = A_i^{eff}/A_d$. For each of these hotspots (j) nucleation depends on the parameter R_i for the node exceeding the local nucleation strength $R_{c,j}$, which occurs with probability $P(R_i > R_{c,j})$. The probability of nucleation around the node i is then calculated as $P_i^{nucl} = 1 - \prod_{j=1}^{N_i} P(R_i < R_{c,j})$, where the nucleation strength $R_{c,j}$ of each hotspot j is an independent and identically distributed (*IID*) random variable. P_i^{nucl} is the distribution corresponding to the minimum of N *IID* random variables and is an extreme value distribution. For a large number of dislocation pile-ups impinging on the hard grain ($N_i \gg 1$), a two-parameter Weibull distribution [29] is found to best represent the probability of nucleation around the node, i.e. $P_i^{nucl} = 1 - e^{-\left(\frac{R_i}{R_{c0}}\right)^k N_i}$. Here k is the Weibull modulus controlling the variance of the distribution and R_{c0} is a characteristic nucleation strength parameter. The deterministic model in Eq. (1) [1] is recovered in the limit as $k \to \infty$. The probability of crack nucleation at a soft-hard grain boundary (GB) is equal to the probability of any of the wedge cracks opening up into the hard grain. This is calculated as:

$$P_{GB}^{nucl} = 1 - e^{-\left(\frac{R_1}{R_{c0}}\right)^k N_1} \cdots e^{-\left(\frac{R_{n_{GB}}}{R_{c0}}\right)^k N_{n_{GB}}} = 1 - \exp\left[-\sum_{i=1}^{n_{GB}} \left(\frac{R_i}{R_{c0}}\right)^k \frac{A_i^{eff}}{A_d}\right] \quad (2)$$

where n_{GB} is the number of nodes on the boundary of the hard-soft grain pair. A high probability (~90–95%) in Eq. (2) is assumed to indicate the crack nucleation at a given microstructural point. The image-based CPFE simulations are compared with experimental observations to calibrate parameters in the constitutive and crack nucleation models.

5. Image-based CPFE simulations for crack nucleation with potential facet formation

A SERVE of the polycrystalline microstructure of the Ti-7Al alloy with 307 grains is generated as described in the experimental section, and is meshed with 136,466 linear 4-noded tetrahedral elements as shown in Fig. 2(a). WATMUS-accelerated CPFE simulations are performed under four different loading cases, viz. dwell and cyclic loading with peak stress $\mathbf{P_{max}}$ equal to either 85% or 100% of the macroscopic yield stress of the polycrystalline model (662 MPa), following the experimental loading profiles. The nucleation model parameters R_{c0}, N_c and k are calibrated from experimentally observed nucleation lifetimes for the loading cases: dwell and cyclic loading at $\mathbf{P_{max}} = 100\%$Y.S., and dwell loading at $\mathbf{P_{max}} = 85\%$Y.S. The calibrated values are: $R_{c0} = 13.17\ \mathrm{MPa.\mu m^{1/2}}$, $k = 6$ and $N_c = 8862$. The model is then used to predict the number of cycles to nucleation under cyclic loading at $\mathbf{P_{max}} = 85\%$Y.S. Table 1 and Fig. 2(c) compares the calibrated and predicted number of cycles to crack nucleation with the experimentally observed values for the four loading cases. The purely predicted nucleation lifetime of $N = 36{,}352$ is within 15% of the experimentally observed value of 43,000. Nucleation lives at $\mathbf{P_{max}} = 90\%$Y.S. and 95%Y.S. are also evaluated and plotted in Fig. 2(c) to study the general trend of the nucleation life as a function of $\mathbf{P_{max}}$. The simulated dwell debits for crack nucleation are in very good agreement with the experiments and are also consistent with those reported in the literature on α, near-α and α/β titanium alloys [3,6,30].

The probabilistic nucleation model is also validated with experimental observations for critical facet orientations. After determining the critical crack plane normal $\hat{\mathbf{n}}_i^{cra}$ and probability of nucleation P_i^{nucl} at each node i, $\hat{\mathbf{n}}_i^{cra}$ is stereographically projected on the specimen frame. The projection space is divided into a grid of bins as shown in Fig. 3(a), each one covering one neighborhood of crack orientations.

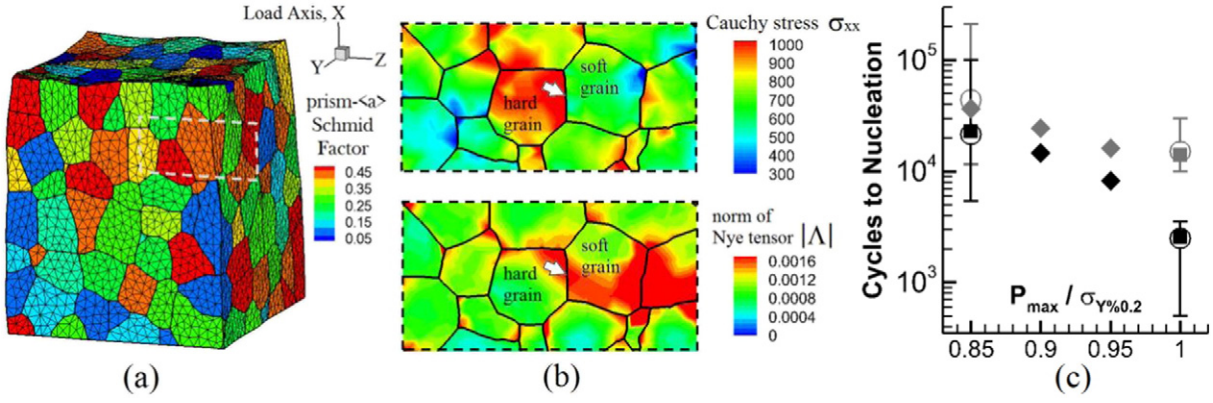

Fig. 2. (a) Statistically equivalent polycrystalline Ti-7Al model showing the Schmid factor contour plot, (b) cross section showing stress and Nye tensor fields around a critical soft-hard grain pair after 2824 cycles of dwell loading at $\mathbf{P_{max}} = 100\%$Y.S., (c) number of cycles to crack initiation under dwell (black) and cyclic loading (grey) and $\mathbf{P_{max}}$ varying from 85%Y.S. to 100%Y.S. Circles and error bars: experimental mean and fracture-mechanics-estimated bounds of nucleation life. Squares and diamonds: calibrated and predicted number of cycles to nucleation, respectively.

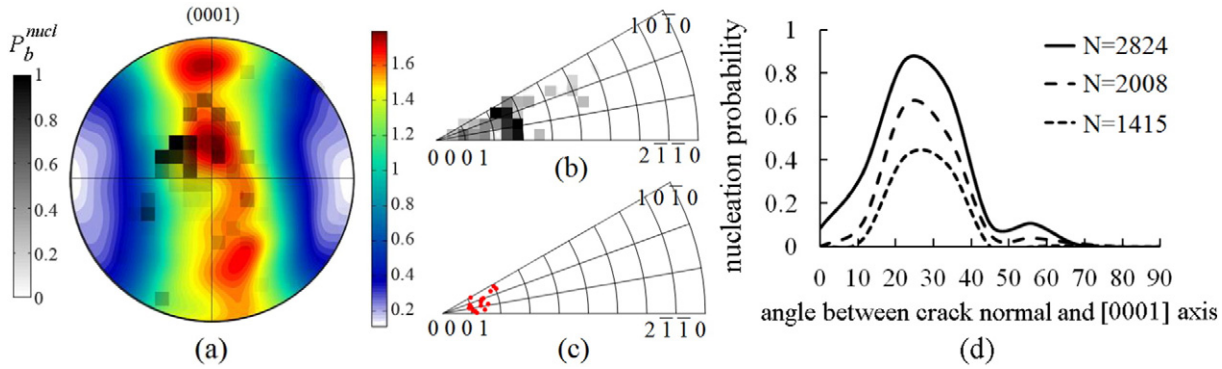

Fig. 3. Simulation-based probability distributions of crack orientations (P_b^{nucl}, greyscale) plotted in: (a) a global reference system overlaid on (0001) pole figure (color), and (b) the crystal frame as IPF, at 2824 cycles, for dwell loading with $\mathbf{P_{max}} = 100\%$Y.S., (c) IPF of observed facet normals near initiation site, and (d) simulated nucleation probabilities as a function of the angle between crack normal and [0001] axis.

The probability of finding a crack oriented within each bin b is calculated as $P_b^{nucl} = 1 - \prod_{j=1}^{N_b}[1 - P_j^{nucl}]$, where N_b is the number of crack plane normals projected onto bin b.

The probability of nucleation for each orientation in the specimen coordinate frame are calculated after 2824 cycles of dwell loading at $\mathbf{P_{max}} = 100\%$ YS and plotted in Fig. 3(a). This shows the distribution of crack orientations with high cracking potential with respect to the sample reference frame. The simulated and experimental data show that the group of grains with c-axes inclined at 10°–50° to the stress axis are the most potent nucleation sites. To obtain a complete description of facet crystallography, inverse pole figures (IPF) of nucleation probabilities are evaluated, by first transforming each crack plane normal $\hat{\mathbf{n}}_i^{cra}$ onto the unit triangle of the *hcp* crystal lattice, and subsequently following the same binning procedure described above. The probability of nucleation as a function of crystallographic orientation is plotted in Fig. 3(b). This result is compared to a set of experimentally observed facet surface crystallographic orientations in Fig. 3(c). The probability of nucleation as a function of the angle between facet normal and the crystallographic [0001] axis is plotted in Fig. 3(d) with increasing number of cycles, showing a range ~10–30°, with a peak near 25°. While the model does not introduce an explicit bias with respect to the fracture plane, Fig. 3(b) and (d) clearly illustrate that it correctly predicts a cluster of facet planes that also encompasses the frequent experimental observation of fracture planes inclined ~15° from the (0001) direction (Fig.3(c)).

6. Conclusions

This paper develops a promising image-based crystal plasticity finite element model in conjunction with a probabilistic crack nucleation model for predicting fatigue crack nucleation in polycrystalline microstructures of Ti alloys under both dwell and cyclic loading. The fatigue nucleation model accounts for load-shedding phenomena due to time-dependent plastic flow in soft grains, as well as the variability in crystal strength due to underlying crystallographic defects at a lower length-scale. While the microstructure sampled is only slightly micro-textured, the effect of micro-texture on load-shedding is replicated by large grains contiguous to smaller sized grains [25]. The overall modeling framework has good predictive capabilities that are corroborated with experimental observations of facet nucleation for cyclic and dwell loading, at peak stresses of 85% to 100% of YS. The cycles to nucleation vary from 2500 to 43,000. The predicted reduction in dwell debit with peak stresses under ~90% of YS is consistent with experimental observations in [3,6,30]. At higher peak stresses, time-dependent load shedding mechanism dominates, introducing a significant dwell debit, while limited dependence on stress hold is observed at lower peak stresses. Finally, the simulated probability distribution of crack plane orientations reveals the critical crystallographic orientations for nucleation. They are in excellent agreement with experimentally measured orientations of faceted cracks at initiation sites.

Acknowledgements

This work is supported through a subcontract to JHU (sub-recipient) from the Ohio State University (main recipient) through a sub-award No. 60038238 from an AFRL grant No. FA8650-13-2-2347 as a part of the AFRL Collaborative Center of Structural Sciences. The program managers of this grant are Dr. B. Smarslok and Dr. R. Chona, and the PI is Prof. J. McNamara. This support to JHU is gratefully acknowledged. Computer use of the Hopkins High Performance Computing facilities is gratefully acknowledged. Adam Pilchak gratefully acknowledges the support of AFOSR Task No. 12RX01COR, with program manager Dr. A. Sayir.

References

[1] M. Anahid, M.K. Samal, S. Ghosh, J. Mech, Phys. Solids 59 (2011) 2157–2176.
[2] S. Ghosh, P. Chakraborty, Int. J. Fatigue 48 (2013) 231–246.
[3] M. Bache, Int. J. Fatigue 25 (2003) 1079–1087.
[4] V. Sinha, J.E. Spowart, M.J. Mills, J.C. Williams, Metall. Mater. Trans. A 37 (2006) 1507–1518.
[5] V. Sinha, M.J. Mills, J.C. Williams, J. Mater. Sci. 42 (2007) 8334–8341.
[6] V. Sinha, M.J. Mills, J.C. Williams, Metall. Mater. Trans. A 35 (2004) 3141–3148.
[7] Z. Zhang, M.A. Cuddihy, F.P.E. Dunne, Proc. R. Soc. A Math. Phys. Eng. Sci. 471 (2015), 20150214.
[8] Z. Zhang, T.-S. Jun, T.B. Britton, F.P.E. Dunne, J. Mech, Phys. Solids 95 (2016) 393–410.
[9] T.-S. Jun, Z. Zhang, G. Sernicola, F.P.E. Dunne, T.B. Britton, Acta Mater. 107 (2016) 298–309.
[10] T. Neeraj, M. Mills, Mater. Sci. Eng. A 319-321 (2001) 415–419.
[11] J.C. Williams, R.G. Baggerly, N.E. Paton, Mater. Trans. a-Physical Metall. Mater. Sci. 33 (2002) 837–850.
[12] Y. Guo, T.B. Britton, A.J. Wilkinson, Acta Mater. 76 (2014) 1–12.
[13] M.D. Sangid, T. Ezaz, H. Sehitoglu, I.M. Robertson, Acta Mater. 59 (2011) 283–296.
[14] T.C. Lee, I.M. Robertson, H.K. Birnbaum, Metall. Trans. A 21 (1990) 2437–2447.
[15] A.L. Pilchak, J.C. Williams, Metall. Mater. Trans. A 42 (2011) 1000–1027.
[16] A.L. Pilchak, M.C. Brandes, R.E.A. Williams, J.C. Williams, Ti-2011, 2011 1–4.
[17] S.I. Rokhlin, J.-Y. Kim, B. Xie, B. Zoofan, NDT E Int. 40 (2007) 462–470.
[18] J.C. Williams, The Evaluation of Cold Dwell Fatigue in Ti-6242, 2006.
[19] M.H. Pourian, F. Bridier, P. Pilvin, P. Bocher, Int. J. Fatigue 85 (2016) 85–97.
[20] C.P. Przybyla, D.L. McDowell, Int. J. Plast. 27 (2011) 1871–1895.
[21] A.L. Pilchak, Scr. Mater. 74 (2014) 68–71.
[22] M. Groeber, S. Ghosh, M.D. Uchic, D.M. Dimiduk, Acta Mater. 56 (2008) 1257–1273.
[23] V. Hasija, S. Ghosh, M.J. Mills, D.S. Joseph, Acta Mater. 51 (2003) 4533–4549.
[24] D. Deka, D.S. Joseph, S. Ghosh, M.J. Mills, Metall. Mater. Trans. A 37 (2006) 1371–1388.
[25] G. Venkatramani, S. Ghosh, M. Mills, Acta Mater. 55 (2007) 3971–3986.
[26] F.P.E. Dunne, D. Rugg, A. Walker, Int. J. Plast. 23 (2007) 1061–1083.
[27] D.S. Joseph, P. Chakraborty, S. Ghosh, Comput. Methods Appl. Mech. Eng. 199 (2010) 2177–2194.
[28] A.N. Stroh, Proc. R. Soc. A Math. Phys. Eng. Sci. 223 (1954) 404–414.
[29] R.A. Fisher, L.H.C. Tippett, Math. Proc. Camb. Philos. Soc. 24 (1928) 180–190.
[30] M.E. Kassner, Y. Kosaka, J.S. Hall, Metall. Mater. Trans. A 30 (1999) 2383–2389.